Electrochemical Performance of $Li_xMn_{2-y}Fe_yO_{4-z}Cl_z$ Synthesized Through In-Situ Glycine Nitrate Combustion

Ashley L. Ruth, Paula C. Latorre, and Terrill B. Atwater
U.S. Army Communications Electronics Research Development and Engineering Center
Power Division – Command Power and Integration
Aberdeen Proving Ground, MD, USA, 21005

Abstract: *Lithium manganese oxide spinel is an attractive material for lithium-ion battery cathodes due to its 3D network of lithium pathways within the structure. However, this material suffers from limited cyclability as a result of structural decomposition through extended lithium insertion and deinsertion cycling. This is due to the energy barriers for removing lithium from the octahedral sites as well as the formation of Mn^{3+} ions via the Jahn-Teller effect. The use of the glycine nitrate combustion synthesis produces small particles at reduced time and temperature during the calcining step of the synthesis process, which affords a uniform introduction of a Fe B-site modifier of AB_2O_4. This work incorporates chlorine to form more polarized Metal-Cl bonds to assist with liquid to solid transfer of Li^+ during the initial Fe-doping synthesis; this allows total production time to be achieved in less than 8 hours, preventing extended calcining times and at elevated temperatures which cause defect association leading to phase separation. These electrochemical cells cycle between 4.5 V and 3.5 V at 1.0 mA cm^{-2} (10 mA g_{active}^{-1}) and achieve over 250 cycles, maintaining 98% of original discharge at 71 mAh g^{-1}. Additionally, when cycled to a deeper potential at 2.25 V the electrochemical cell delivered a capacity of 142 mAh g^{-1} and is completely reversible without negatively impacting further cycling. This performance allows for access to energy at extended cycling and across potential regimes.*

Keywords: Li-ion battery; Lithium manganese oxide spinel; spinel cathode; Fe-doping; secondary lithium battery

Introduction

High voltage lithium manganese oxide spinels have been utilized in cathode materials for lithium-ion batteries due to their affordability and low toxicity while maintaining reasonable capacity [1-3]. However, this spinel suffers from capacity fading as a result of structural degradation either through the Jahn-Teller distortion, alternative phase formation via non-stoichiometry, or loss of crystallinity [4-6]. In an effort to combat these concerns, cycle life improvements have been achieved through stabilization of the spinel structure via transition metal doping on the B-site of the AB_2O_4 lattice [7-15]. The transition metal iron is a suitable dopant because of its low toxicity, but primarily due to affordability. Iron also has a high voltage redox couple of Fe^{3+} and Fe^{4+} at ~ 5.1 V allowing for high voltage applications [16-19]. Taniguchi and Bakenov demonstrate an increased capacity retention of $LiMn_{2-x}Fe_xO_4$ versus the undoped $LiMn_2O_4$ spinel over 100 cycles using a flame pyrolysis synthesis method [20].

While B-site doping has improved cyclability, adding anion dopants could enhance cycle life in $Li_xMn_{2-y}Fe_yO_4$ (LMFO). Our group as well as other researchers have added chlorine and more commonly fluorine and demonstrated performance enhancements [9, 13-14, 21-24]. However, many studies tend to coat the halide onto the surface of the spinel rather than incorporating it homogenously into the lattice. Liu et al. prepared a homogenous $LiMn_2O_{4-z}Cl_z$ material via a citrate gel method that demonstrated promising results [24]. Unfortunately only 10 charge/discharge cycles were reported. With regard to fluorine addition, Son and Kim as well as Amatucci et al. show an improvement in capacity with fluorine doping, however the discharge capacity rapidly declines resulting in short cycle life [14, 23].

This work intends to study the impact of adding the less common chlorine anion dopant on the cyclability of the B-site doped $Li_xMn_{2-y}Fe_yO_4$ material. By taking advantage of submicron ceramic synthesis, namely the glycine nitrate combustion process (GNP), we propose the capability for *in-situ* B-site doping and anion doping to synthesize the $Li_xMn_{2-y}Fe_yO_{4-z}Cl_z$ material.

Experimental

A glycine nitrate combustion method was used to synthesize iron doped chlorinated lithium manganese oxide spinel (LMFO-Cl). Stoichiometric amounts of $Li(NO_3)$ and $Mn(NO_3)_2{\cdot}4H_2O$ (Alfa Aesar) with $FeCl_3$ were mixed to incorporate both the iron and chlorine content then dissolved in DI H_2O. NH_2CH_2COOH (glycine, Alfa Aesar) was dissolved into the aqueous solution as a chelating agent in a 1:1 metal-ion to glycine ratio. The solution was heated to 80°C until the water fully evaporated and a gel was formed. The gel was heated further to 250°C when auto ignition occurs and formed a black ash. The ash was collected and ground in a mortar and pestle and fired at 600°C for two hours to achieve the desired phase.

Phase purity was determined using x-ray diffraction (XRD, Bruker D8 Advance, Cu-kα. chlorine content was determined from x-ray fluorescence spectroscopy (XRF, Bruker S2 Ranger) after firing for phase formation. Experimental button cells were assembled using a lithium

anode separated from the cathode by a 0.01 cm nonwoven glass separator. $Li_xMn_{2-y}Fe_yO_{4-z}Cl_z$ cathode was fabricated by mixing together the active material, carbon, and polytetrafluoroethylene (PTFE) in an 85:10:5 by weight ratio, respectively. The cathode mixture was rolled to 0.04 cm and dried in a vacuum oven. A 0.075 cm thick lithium foil was cut using a 12.7 mm hole punch. The cathode was cut into 1.0 cm^2 discs of approximately 0.13 g. The electrolyte used was 1 molar $LiPF_6$ in a proportional mixture of diethyl carbonate, dimethyl carbonate, and ethylene carbonate.

Cells were cycled with an ARBIN MSTAT4 battery cycler system controlled by MITS Pro software. The cells were charged and discharged from 4.5 V to 3.5 V, 4.5 V to 2.25 V, or 4.75 V to 3.5 V. The charge/discharge rates were maintained at 1.0 mA cm^{-2} or 2.0 mA cm^{-2}. A rest period of 15 minutes between charge and discharge cycles was used to allow for cells to achieve equilibrium on all experiments.

Results and Discussion

In order to confirm correct phase formation, XRD was performed on the $Li_xMn_{2-y}Fe_yO_{4-z}Cl_z$ cathode material after calcination. Figure 1 shows the resultant diffraction spectrum as compared with the JCPDS file for $LiMn_2O_4$ spinel (PDF 01-070-3120). While a slight shift is expected due to the iron dopant, no additional peaks are detected, indicating relative phase purity with no secondary phases that may not participate electrochemically.

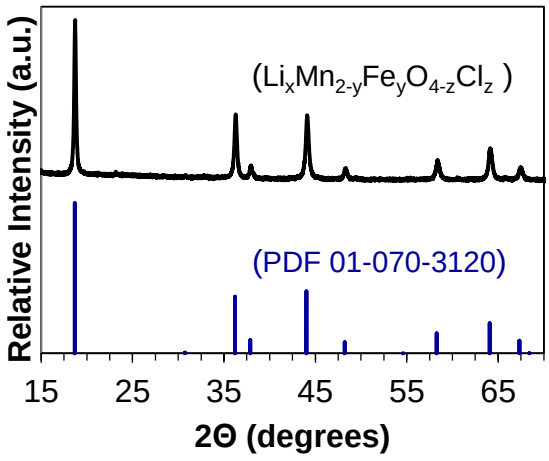

Figure 1. X-ray diffraction results for $Li_xMn_{2-y}Fe_yO_{4-z}Cl_z$ cathode material as compared with JCPDS file (PDF 01-070-3120) for $LiMn_2O_4$ spinel.

The energetic nature of the ignition synthesis method or the calcination process could have resulted in loss of the chlorine dopant. In order to address this concern, the $Li_xMn_{2-y}Fe_yO_{4-z}Cl_z$ cathode material was observed using XRF to confirm the maintenance of chlorine after the calcination to the correct phase is complete. Figure 2 shows the elemental components of the calcined material. Si, P, and S are expected background due to the polymer sample holder. The Pd peaks are the signature of the Pd x-ray source. As expected, there is very high (off the chart) intensity for the Mn and Fe peaks. Due to overlap, the Fe is confirmed by the Kb1 emission 7.06 keV. Most importantly, the Cl peak is clearly discernable, showing the presence of chlorine in the $Li_xMn_{2-y}Fe_yO_{4-z}Cl_z$ material after calcination.

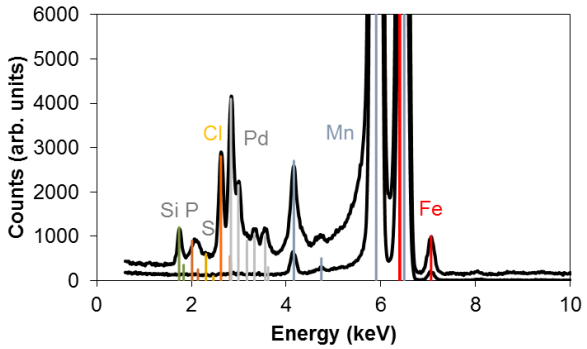

Figure 2. X-ray fluorescence results for the $Li_xMn_{2-y}Fe_yO_{4-z}Cl_z$ cathode material.

Electrochemical measurements were performed on the $Li_xMn_{2-y}Fe_yO_{4-z}Cl_z$ cathode material opposite a Li metal anode and results are shown in Figures 3-5 for y = 0.195 and z = 0.028. In Figure 3, the coulombic efficiency and charge and discharge capacities are shown up to 250 cycles. Beyond 250 cycles the periodic shorting indicated by overcharge data points worsens. However, the discharge capacity at cycle 250 is still greater than 98% of the original discharge capacity, demonstrating a very long cycle life.

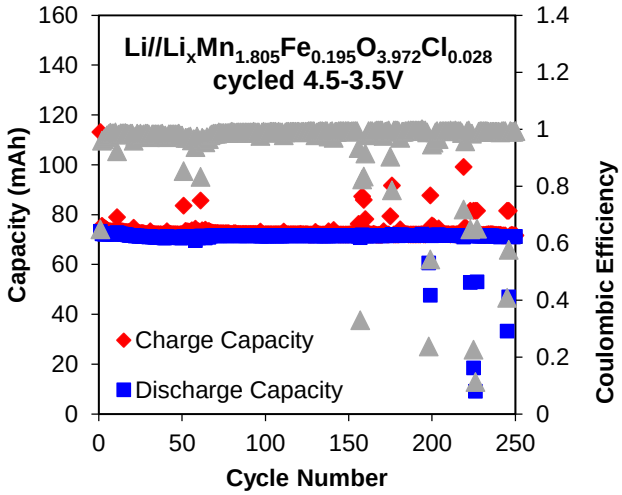

Figure 3. Specific capacity (bottom) and coulombic efficiency (top) during 250 charge/discharge cycles of a $Li_xMn_{2-y}Fe_yO_{4-z}Cl_z$ experimental button cell where y = 0.195 and z = 0.028.

The periodic shorting shown in Figure 3 is not a desirable characteristic for cells in operation, but these shorts are a result of the laboratory scale cell fabrication. The separator is a nonwoven glass separator that acts as a wick rather than a true separator that could prevent shorting through dendritic growth. So the lithium can easily form whiskers and subsequent cycling can grow them long enough to short. Once the short is alleviated, the cell returns to normal cycling behavior.

A differential capacity curve was generated from the charge/discharge data at several cycles to observe the changes over time. The resultant data is shown in Figure 4. The electrochemical peaks begin to shift in voltage and exhibit peak broadening. This shift could be due either electrolyte degradation or a breakdown of the spinel structure of the cathode. However, because the capacity remains intact through cycling, it is unlikely that the cathode is suffering from structural degradation. $LiPF_6$ electrolytes are known to degrade at high voltages (greater than 4.5V) and is a well-known culprit for poor extended performance in high voltage lithium-ion battery cathodes [25-26]. Therefore, the spinel chemistry is demonstrated to be robust enough for extended cycling should a suitable electrolyte be used.

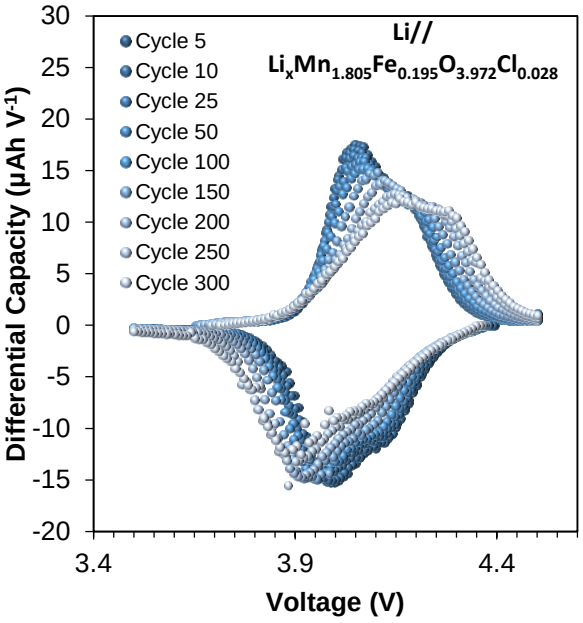

Figure 4. Differential capacity curves for cycles 5, 10, 25, 50, 100, 150, 200, 150, and 300 of a $Li_xMn_{2-y}Fe_yO_{4-z}Cl_z$ experimental cell for y = 0.195 and z = 0.028.

Beyond 250 cycles, an attempt to discharge the experimental cell below 3.5 V to 2.25 V was made in order to determine if there is any vulnerability of the cell at this deep discharge. This was performed at cycle 286 and is shown in Figure 5. Cycles 299 and 300 cycled from 4.5 V to 3.5 V and are also shown in Figure 5. These cycles are comparable to the deeper discharge of cycle 286 in the 4.5 V to 3.5 V regime, as expected. However, the fact that cycles 299 and 300 exist is a testament to the ability of this chemistry to withstand significant lithium insertion and still continue to cycle in the normal operating regime at 98% of original discharge capacity at 71 mAh/g. During the deep discharge to 2.25 V at cycle 286, a discharge capacity of 142 mAh/g is achieved. This is twice that of the upper voltage regime, as expected from the chemistry of inserting an additional lithium into the spinel cathode lattice.

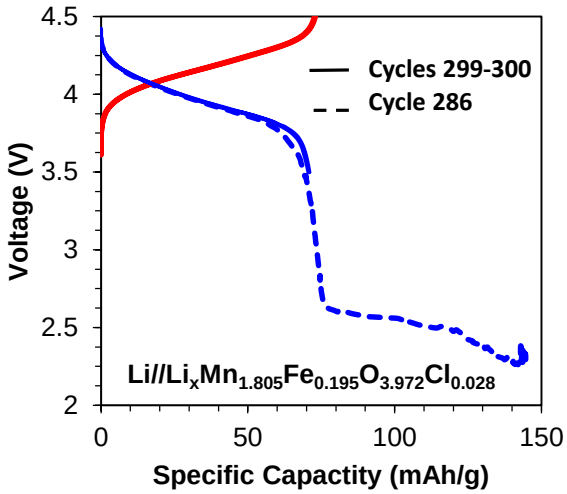

Figure 5. Charge (red) /discharge (blue) curves for cycles 286, 299, and 300 of an $Li_xMn_{2-y}Fe_yO_{4-z}Cl_z$ experimental cell for y = 0.195 and z = 0.028. A solid line indicates 4.5 V to 3.5 V cycling, and dashed lines indicates a full deep discharge to 2.25 V at 2.0 mA/cm^2.

Conclusions

A high voltage capable $Li_xMn_{2-y}Fe_yO_{4-z}Cl_z$ spinel cathode material was synthesized using very fast processing times taking advantage of the high energy precursor formation from the glycine nitrate combustion reaction. This allowed for a very short 2 hour calcination at just 600 °C to form the correct phase while retaining the chlorine addition. Testing this $Li_xMn_{2-y}Fe_yO_{4-z}Cl_z$ cathode material in an electrochemical cell opposite a lithium metal anode resulted in excellent cycle life up to 250 cycles and beyond with greater than 98% of the original discharge capacity. Future work would include incorporating a more robust separator as well as a high voltage electrolyte that will not degrade at advanced cycling at high voltages. More research is needed for selecting the appropriate high voltage electrolyte for this system. Should an adequate electrolyte be used in addition to a separator that can prevent dendritic shorts, an even greater cycle life of this $Li_xMn_{2-y}Fe_yO_{4-z}Cl_z$ cathode chemistry may be realized.

References

[1] H. Xia, Y.S. Meng, M.O. Lai, L. Lu, Journal of The Electrochemical Society, 157 (2010) A348-A354.
[2] B. Ebin, S. Gürmen, C. Arslan, G. Lindbergh, Electrochimica Acta, 76 (2012) 368-374.
[3] D. Liu, W. Zhu, J. Trottier, C. Gagnon, F. Barray, A. Guerfi, A. Mauger, H. Groult, C.M. Julien, J.B. Goodenough, K. Zaghib, RSC Advances, 4 (2014) 154-167.
[4] H. Xia, Z. Luo, J. Xie, Progress in Natural Science: Materials International, 22 (2012) 572-584.
[5] H. Huang, C.A. Vincent, P.G. Bruce, Journal of The Electrochemical Society, 146 (1999) 3649-3654.
[6] Y. Xia, M. Yoshio, Journal of The Electrochemical Society, 143 (1996) 825-833.
[7] N.M. Hagh, G.G. Amatucci, Journal of Power Sources, 256 (2014) 457-469.
[8] S. Jayapal, R. Mariappan, S. Sundar, S. Piraman, Journal of Electroanalytical Chemistry, 720 (2014) 58-63.
[9] X. He, J. Li, Y. Cai, Y. Wang, J. Ying, C. Jiang, C. Wan, Journal of Power Sources, 150 (2005) 216-222.
[10] J. Morales, L. Sánchez, J. Tirado, Journal of Solid State Electrochemistry, 2 (1998) 420-426.
[11] J. Amarilla, J. Martin de Vidales, R. Rojas, Solid State Ionics, 127 (2000) 73-81.
[12] H.J. Bang, V. Donepudi, J. Prakash, Electrochimica Acta, 48 (2002) 443-451.
[13] G. Amatucci, A. Du Pasquier, A. Blyr, T. Zheng, J.-M. Tarascon, Electrochimica Acta, 45 (1999) 255-271.
[14] G. Amatucci, N. Pereira, T. Zheng, I. Plitz, J. Tarascon, Journal of Power Sources, 81 (1999) 39-43.
[15] C. Wu, F. Wu, L. Chen, X. Huang, Solid State Ionics, 152 (2002) 335-339.
[16] A. Eftekhari, Journal of Power Sources, 124 (2003) 182-190.
[17] M. Pico, I. Álvarez-Serrano, M. López, M. Veiga, Dalton Transactions, 43 (2014) 14787-14797.
[18] H. Kawai, M. Nagata, M. Tabuchi, H. Tukamoto, A.R. West, Chemistry of materials, 10 (1998) 3266-3268.
[19] L. Herna, J. Morales, L. Sanchez, E. Rodriguez Castello, and M.A.G. Arandab, *Journal of Materials Chemistry*, 12 (2002) 734–741.
[20] I. Taniguchi, Z. Bakenov, Powder technology, 159 (2005) 55-62.
[21] T. Atwater, P. Tavares, SAE International Journal of Materials and Manufacturing, 6 (2013) 85-89.
[22] T.B. Atwater, P.C. Tavares, in, US Patent 8,900,756, 2014.
[23] J. Son, H. Kim, Journal of Power Sources, 147 (2005) 220-226.
[24] W.-R. Liu, S.-H. Wu, H.-S. Sheu, Journal of Power Sources, 146 (2005) 232-236.
[25] L. Yang, B. Ravdel, B.L. Lucht, Electrochemical and Solid-State Letters, 13 (2010) A95-A97.
[26] L. Hu, Z. Zhang, K. Amine, Journal of Power Sources, 236 (2013) 175-180.